

Cooperative Yb^{3+} - Tb^{3+} dimer excitations and upconversion in $\text{Cs}_3\text{Tb}_2\text{Br}_9:\text{Yb}^{3+}$ G. M. Salley,¹ R. Valiente,² and H. U. Güdel¹¹*Departement für Chemie und Biochemie, Universität Bern, Freiestrasse 3, CH-3000 Bern 9, Switzerland*²*Dept. de Física Aplicada, Facultad de Ciencias, Universidad de Cantabria, 39005 Santander, Spain*

(Received 7 May 2002; revised manuscript received 24 July 2002; published 28 April 2003)

Green $\text{Tb}^{3+} {}^5\text{D}_4 \rightarrow {}^7\text{F}_J$ luminescence visible by eye is observed under near-infrared laser excitation. Optical spectroscopic techniques including absorption, luminescence, and excitation spectroscopy are used to characterize this upconversion (UC) luminescence. The Tb^{3+} UC luminescence is present for all temperatures within a range from 10 to 300 K, and gains intensity by three orders of magnitude between 10 and 300 K. For $T \geq 100$ K the dominant upconversion mechanism is the cooperative sensitization of Tb^{3+} by two Yb^{3+} ions. In this temperature regime the Tb^{3+} UC luminescence dominates the visible (VIS) spectrum for all near-infrared (NIR) excitations, resulting in the characteristic green luminescence. At 10 K, the color of the luminescence changes from green to blue, depending on the excitation wavelength corresponding to the dominance of Tb^{3+} UC luminescence or the Yb^{3+} - Yb^{3+} cooperative pair luminescence. Two color excitation spectroscopy is performed to directly observe an excited state absorption (ESA) step in the Tb^{3+} UC luminescence excitation spectrum at 10 K. This allows the unambiguous assignment of a type of ground state absorption/excited state absorption (GSA/ESA) mechanism responsible for the upconversion in this system at 10 K. We explain this cooperative interaction in the framework of an Yb^{3+} - Tb^{3+} exchange-coupled dimer. An energy level diagram for this dimer is presented. Excitation into dimer levels around $12000\text{--}14500\text{ cm}^{-1}$, where neither Yb^{3+} nor Tb^{3+} single ions have levels, leads to Yb^{3+} luminescence at 10 K. For laser excitation, 53 W/mm^2 , resonant with an ESA transition a VIS/NIR photon ratio of $2.7(10)^{-5}$ is found at 10 K.

DOI: 10.1103/PhysRevB.67.134111

PACS number(s): 78.55.Hx, 75.30.Et

I. INTRODUCTION

The conversion of near-infrared (NIR) photons to visible (VIS) photons has been studied extensively since Auzel first described this phenomenon in 1966.¹ Many papers with fundamental and practical interest have been published on this subject since then. Practical interest in upconversion (UC) materials is found in the fields of solid-state lasers, lamp phosphors, optical data storage, IR counters, and others.² Many fundamental research papers on this subject are also published every year. To improve the efficiency and light yield of UC materials one must understand the mechanism which drives the process.

The mechanisms in mixed UC systems consisting of two different chromophores, such as Yb^{3+} - Tb^{3+} , have historically been assigned to processes involving energy transfer steps.³ The energy transfer steps can occur sequentially, e.g. GSA/ETU (ground state absorption/energy transfer upconversion), or simultaneously, e.g. cooperative sensitization.^{4,5} These processes can be extremely efficient and some UC laser systems have been created using this principle.²

A recent report demonstrated a UC process for the mixed Yb^{3+} - Mn^{2+} system.⁶⁻⁸ It was assigned to a mechanism based on exchange interactions between the Yb^{3+} rare-earth (RE) ion and the Mn^{2+} transition metal ion. A sequence of GSA and ESA steps on an Yb^{3+} - Mn^{2+} dimer was found to be important, and is the first observation of a GSA/ESA mechanism in a mixed UC system. Further studies on similar compounds revealed a dependence of the efficiency of the upconversion process on the Yb^{3+} - Mn^{2+} bridging geometry.^{11,9,10}

The intriguing aspect of UC in the Yb^{3+} - Tb^{3+} system is that there is no possibility for direct one-step energy transfer

between the ions due to a large separation of relevant energy levels.¹² Although some reports in the past have postulated a GSA/ESA type mechanism for Yb^{3+} - Tb^{3+} , no clear evidence has been presented.^{13,14} Most studies have assigned the UC in the Yb^{3+} - Tb^{3+} system to the cooperative sensitization mechanism, which was first proposed in 1969.¹⁵⁻²¹ Recently, a temperature dependent study demonstrated that in many Yb^{3+} - Tb^{3+} systems this process must be mediated by phonons to bridge the electronic energy gap between the $\text{Tb}^{3+} {}^5\text{D}_4$ level and two times the lowest crystal field level of $\text{Yb}^{3+} {}^2\text{F}_{5/2}$.^{22,23}

We have chosen to study $\text{Cs}_3\text{Tb}_2\text{Br}_9:\text{Yb}^{3+}$ because of the dimer nature of the structure (see Fig. 1 Sec. IV), and because previous reports have demonstrated an exchange interaction between RE ions in the pure $\text{Cs}_3\text{Tb}_2\text{Br}_9$ and $\text{Cs}_3\text{Yb}_2\text{Br}_9$.^{24,25} Also, no evidence or trace Er^{3+} impurity luminescence was found, eliminating problems which confused the interpretation of the UC mechanism in earlier studies.^{22,23,26}

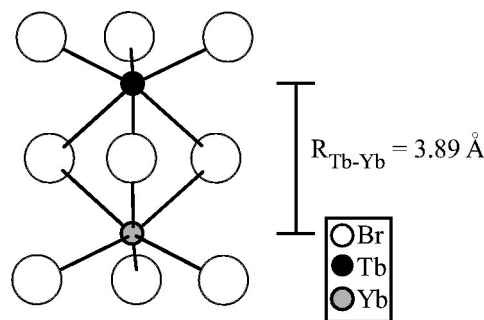


FIG. 1. Relevant dimeric unit of the $\text{Cs}_3\text{Tb}_2\text{Br}_9$ structure. Tb and Yb are contained in face-sharing octahedra.

We present spectroscopic results which allow a clear assignment of the dominant UC process in $\text{Cs}_3\text{Tb}_2\text{Br}_9:\text{Yb}^{3+}$ to a cooperative GSA/ESA dimer mechanism at 10 K and to a cooperative sensitization mechanism at 300 K. At 10 K the ESA step is observed directly through two-color excitation spectroscopy. An enhancement of the UC luminescence efficiency is demonstrated by choosing an excitation energy which is resonant with an ESA transition. We also observe excitation lines from 12000 to 14500 cm^{-1} at 10 K which lead to Yb^{3+} luminescence. These lines are assigned to transitions of the $\text{Yb}^{3+}-\text{Tb}^{3+}$ dimer with oscillator strengths which are four orders of magnitude weaker than single ion transitions. In the following sections we use single-ion notation to designate energy levels and transitions, until we change to dimer notation in Sec. IV C.

II. EXPERIMENTAL TECHNIQUES

A. Synthesis

Single crystals of Yb^{3+} (1%) doped $\text{Cs}_3\text{Tb}_2\text{Br}_9$ were grown by the Bridgeman technique. The TbCl_3 and YbCl_3 starting materials were prepared from Tb_4O_7 (99.9999%), Yb_2O_3 (99.9999%), NH_4Cl (>99.9%), and HCl (47%) by the ammonium halide method.^{27,28} At all stages of growth and handling the samples were kept in an inert atmosphere of either vacuum, He, or N_2 , to prevent the adsorption of water. Absorption measurements were performed on an unoriented 0.1-cm-long clear crystal, which was sealed in a copper cell with optical windows filled with He gas. Samples for luminescence measurements were sealed in quartz ampoules with a partial atmosphere of He gas.

B. Spectroscopy

The absorption spectra were recorded on a Cary 5e spectrophotometer coupled with a closed-cycle cryogenic refrigerator (Varian) for cooling. Cooling for luminescence measurements was achieved via quartz He gas flow tubes. The luminescence of the sample was excited via an Ar^+ ion laser (Spectra Physics 2060-10 SA) or with a Ti:sapphire laser (Spectra Physics 3900S), pumped by the same Ar^+ ion laser, for Tb^{3+} luminescence and Yb/UC luminescence, respectively. The emission was dispersed through a 0.85-m double monochromator (Spex 1402) with 500-nm blazed 1200 groves/mm gratings, and detected with a cooled red sensitive photomultiplier tube (Hamamatsu 3310-01). A Stanford Research SR-400 photon counter was used with a PC for data collection. The excitation laser beam was focused using an $f=53\text{ mm}$ lens. The laser power was measured with a power meter (Coherent Labmaster-E). All spectra are presented as photons/sec vs cm^{-1} and are corrected for the throughput of the detection system, the detector response, and for the index of refraction of air.

For excitation spectra, the Ti:sapphire laser was scanned using an inchworm controlled (Burleigh PZ-501) birefringent filter and the wavelength was monitored with a wavemeter (Burleigh WA2100). Two color experiments were performed with two Ti:sapphire lasers, pumped by two Ar^+ ion lasers. The pump laser was fixed at a GSA energy with

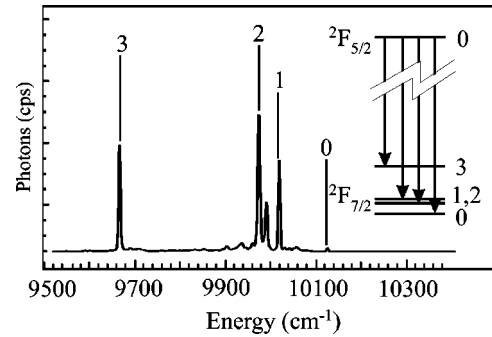


FIG. 2. Yb^{3+} luminescence at 10 K with an excitation energy of 10590 cm^{-1} . The transitions ending on different Stark levels of the $^2\text{F}_{7/2}$ ground state are noted and assigned in the inset.

60 W/mm^2 , and a weak probe laser with 0.25 W/mm^2 was scanned. The Tb^{3+} luminescence was then monitored as a function of the probe laser energy. The spectrum recorded then is an excited state excitation spectrum which is directly related to the excited state absorption.

Kinetic measurements were performed with the same excitation sources described above coupled through an acousto-optical modulator (Coherent 305, Stanford Research DS 345 function generator). The luminescence was dispersed through and detected with the same system as above coupled with a multichannel scaler (Stanford Research SR 430).

III. RESULTS

$\text{Yb}^{3+} \ ^2\text{F}_{5/2} \rightarrow \ ^2\text{F}_{7/2}$ NIR luminescence is plotted in Fig. 2 for $T=10\text{ K}$, and $\tilde{\nu}_{exc}=10590\text{ cm}^{-1}$. The numbers indicate the four electronic origins ending on the four Stark levels 0, 1, 2, and 3, of the $^2\text{F}_{7/2}$ ground state. The transitions are located at 10121 , 10016 , 9972 cm^{-1} , and 9668 cm^{-1} , respectively, and are depicted schematically. The $^2\text{F}_{5/2}(0) \rightarrow \ ^2\text{F}_{7/2}(0)$ origin at 10121 cm^{-1} suffers in intensity from reabsorption. This transition exhibits some vibronic sideband structure. From the origin energies we determine the crystal field levels of the ground state, $^2\text{F}_{7/2}$, found in Table I. Figure 3 displays $\text{Tb}^{3+} \ ^5\text{D}_4 \rightarrow \ ^7\text{F}_j$ emission at $T=10\text{ K}$ for excitation at 20486 cm^{-1} . The numbers in the plot represent transitions ending on different J-multiplets. Each multiplet is further split by the action of the local crystal field, but this is not relevant for this paper and is therefore not discussed. The $^5\text{D}_4 \rightarrow \ ^7\text{F}_5$ is the strongest transition in total emission, yielding a green color seen by eye.

TABLE I. Relevant energy levels of Yb^{3+} and Tb^{3+} and their energies in wave numbers.

Yb^{3+}	$^2\text{F}_{5/2}$	Tb^{3+}	$^5\text{D}_4$
(0) 0	(0) 10121	(0) 20465	(5) 20539
(1) 105	(1) 10148	(1) 20473	(6) 20555
(2) 149	(2) 10590	(2) 20485	(7) 20579
(3) 454		(3) 20508	(8) 20600
		(4) 20519	

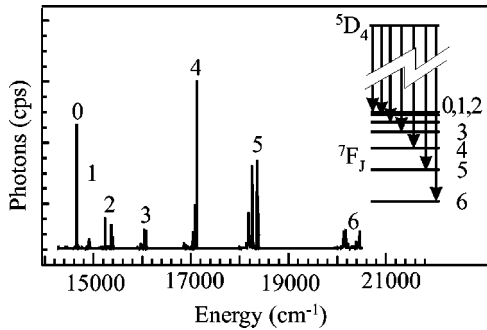


FIG. 3. Tb³⁺ luminescence at 10 K under Ar⁺ excitation, 20486 cm⁻¹. The transitions ending on different J multiplets of the 7F_J manifold are labeled.

Figure 4 plots 10-K Yb³⁺ and Tb³⁺ luminescence intensity on a log scale vs the time after a square wave excitation. The solid data represent the NIR luminescence decay of Yb³⁺, 9972 cm⁻¹, and Tb³⁺, 18193 cm⁻¹, for excitation of 10590 and 20486 cm⁻¹, respectively. The dashed data represent the Tb³⁺ UC luminescence decay after 10357 cm⁻¹ excitation. All three curves are single exponential and the decay rate constants are given in Table II. At 10 K the lifetime of the Yb³⁺ $^2F_{5/2}(0)$ level and the Tb³⁺ $^5D_4(0)$ level are 475 and 916 μ s, respectively.

Visible luminescence spectra under NIR excitation are plotted in Fig. 5, for (a) 300 K, (b) 100 K, and (c) 10 K. The excitation energy for all three plots was resonant with the temperature dependent $^2F_{7/2}(0) \rightarrow ^2F_{5/2}(2)$ transition of Yb³⁺: (a) 10607 cm⁻¹, (b) 10596 cm⁻¹, and (c) 10590 cm⁻¹. All spectra were corrected only for the response of the detection system. The dominant emission in (a) is clearly Tb³⁺ emission. Note that the resolution in this plot is worse than in Fig. 3, resulting in different relative peak heights. At lower temperatures the Tb³⁺ emission is still present but much weaker, and at 10 K Yb³⁺-Yb³⁺ pair luminescence dominates. The inset plots the luminescence ratio of VIS photons divided by NIR photons on a log scale as a function of temperature. The down triangles and squares are for VIS Yb³⁺-Yb³⁺ pair luminescence and VIS Tb³⁺ UC luminescence under NIR $^2F_{7/2}(0) \rightarrow ^2F_{5/2}(2)$ excitation, respectively.

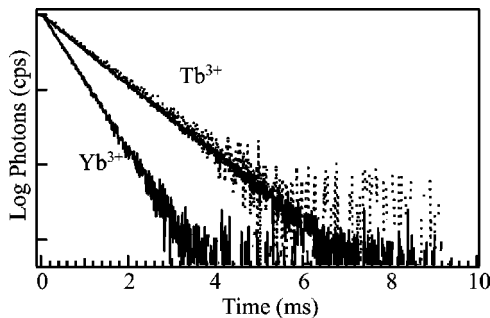


FIG. 4. Log plots of Yb³⁺ (detected at 9972 cm⁻¹) and Tb³⁺ (detected at 18193 cm⁻¹) emission intensities at 10 K after square wave excitation with energies of 10590 and 20486 cm⁻¹, respectively, (solid data). The dashed data represent 10-K Tb³⁺ UC luminescence intensity (detected at 18193 cm⁻¹) after square wave excitation with an energy of 10357 cm⁻¹ at 10 K.

TABLE II. Lifetimes and decay rate constants for Yb³⁺ and Tb³⁺ luminescence at 10 K. The values are taken from fitting the data in Fig. 4 to single exponentials.

Transition	$\tau(\mu\text{s})$	$\kappa(\text{s}^{-1})$	Excitation energy (cm ⁻¹)
Tb ³⁺ ($^5D_4 \rightarrow ^7F_J$)	916	1092	20486
Tb ³⁺ ($^5D_4 \rightarrow ^7F_J$)	971	1030	10357
Yb ³⁺ ($^2F_{5/2} \rightarrow ^2F_{7/2}$)	475	2104	10590

The VIS/NIR photon ratio of the Tb³⁺ UC luminescence has a strong temperature dependence and increases by three orders of magnitude from 10 to 100 K. The VIS/NIR photon ratio increases by four orders of magnitude when exciting at 10364 cm⁻¹. At 10 K in Fig. 5 the Tb³⁺ VIS/NIR ratio is $2(10)^{-5}$, represented by the up triangle, for $\tilde{\nu}_{exc} = 10364$ cm⁻¹. This will be discussed in more detail in Sec. IV C.

The 100-K excitation spectrum in the NIR for Tb³⁺ UC luminescence (detected at 18193 cm⁻¹, solid) and the square of the 100-K Yb³⁺ NIR luminescence excitation spectrum (detected at 9972 cm⁻¹, dashed) are plotted in Fig. 6. The inset plots the same curves expanded by a factor of 6 from 10000 to 10560 cm⁻¹. The transitions to different $^2F_{5/2}$ (i) crystal field levels are labeled as in Fig. 7. Three hot bands, a , b , and c , are observed and will be discussed in Sec. IV B 1.

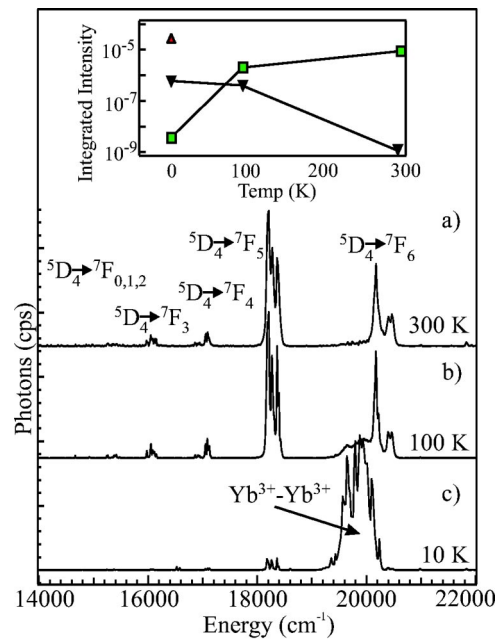


FIG. 5. UC emission spectra at three different temperatures: (a) 300 K, (b) 100 K, and (c) 10 K. The excitation energy for each plot was equal to the temperature dependent Yb³⁺ $^2F_{7/2}(0) \rightarrow ^2F_{5/2}(2)$ transition: (a) 10590 cm⁻¹, (b) 10596 cm⁻¹, and (c) 10607 cm⁻¹. All spectra were corrected for the response of the system only. The inset plots the VIS/NIR photon ratio, described in the text, on a log scale vs temperature, for Yb³⁺-Yb³⁺ pair luminescence (down-triangle), and Tb³⁺ UC luminescence (square). The up-triangle denotes the VIS/NIR photon ratio at 10 K for an excitation resonant with an ESA transition, 10364 cm⁻¹.

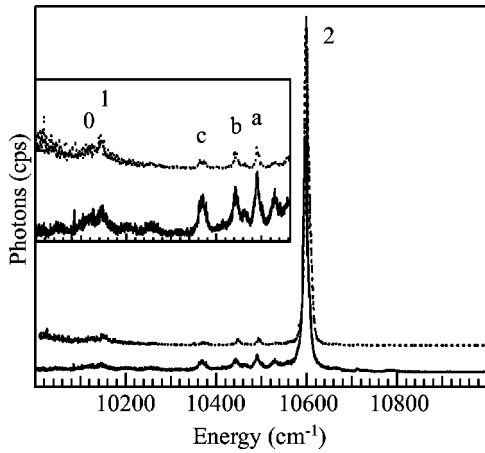


FIG. 6. Excitation spectra in the NIR of Tb^{3+} UC luminescence (detected at 18193 cm^{-1} , solid) and Yb^{3+} luminescence (detected at 9972 cm^{-1} , dashed) at 100 K. The inset plots the same curves from 10000 to 10560 cm^{-1} expanded by a factor of 6. Transitions to the ${}^2F_{5/2}(i)$ levels of Yb^{3+} are labeled. The three peaks a, b, and c, are discussed in Secs. IV B 1 and Sec. IV C.

10-K NIR excitation spectra of Tb^{3+} UC luminescence, detected at 18193 cm^{-1} , and NIR Yb^{3+} luminescence, detected at 9972 cm^{-1} , are plotted in Figs. 7(a) and 7(b), respectively. In (b) transitions to the crystal field levels of the

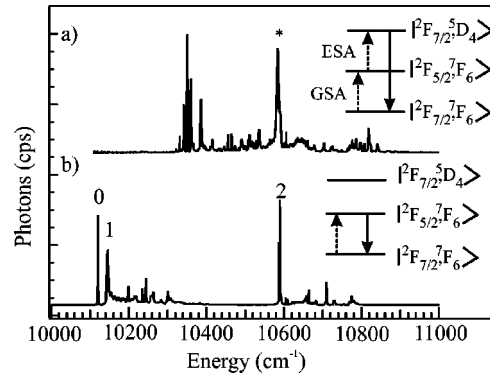


FIG. 7. (a) Excitation spectrum in the NIR of Tb^{3+} UC luminescence at 10 K. (b) Yb^{3+} luminescence excitation spectrum at 10 K. The detection energies were 18193 and 9972 cm^{-1} , respectively. Transitions to the ${}^2F_{5/2}(i)$ levels of Yb^{3+} are labeled in (b). The asterisk denotes the transition ending on the ${}^2F_{5/2}(2)$ level seen in both spectra. The insets show the relevant levels and transitions in Yb^{3+} - Tb^{3+} dimer notation.

${}^2F_{5/2}$ Yb^{3+} multiplet are marked with numbers, and the energetic values can be found in Table I. An asterisk marks the $\text{Yb}^{3+} {}^2F_{7/2}(0) \rightarrow {}^2F_{5/2}(2)$ transition found in the Tb^{3+} UC luminescence excitation spectrum, while the other two Yb^{3+} transitions are clearly absent in (a). Many other lines are

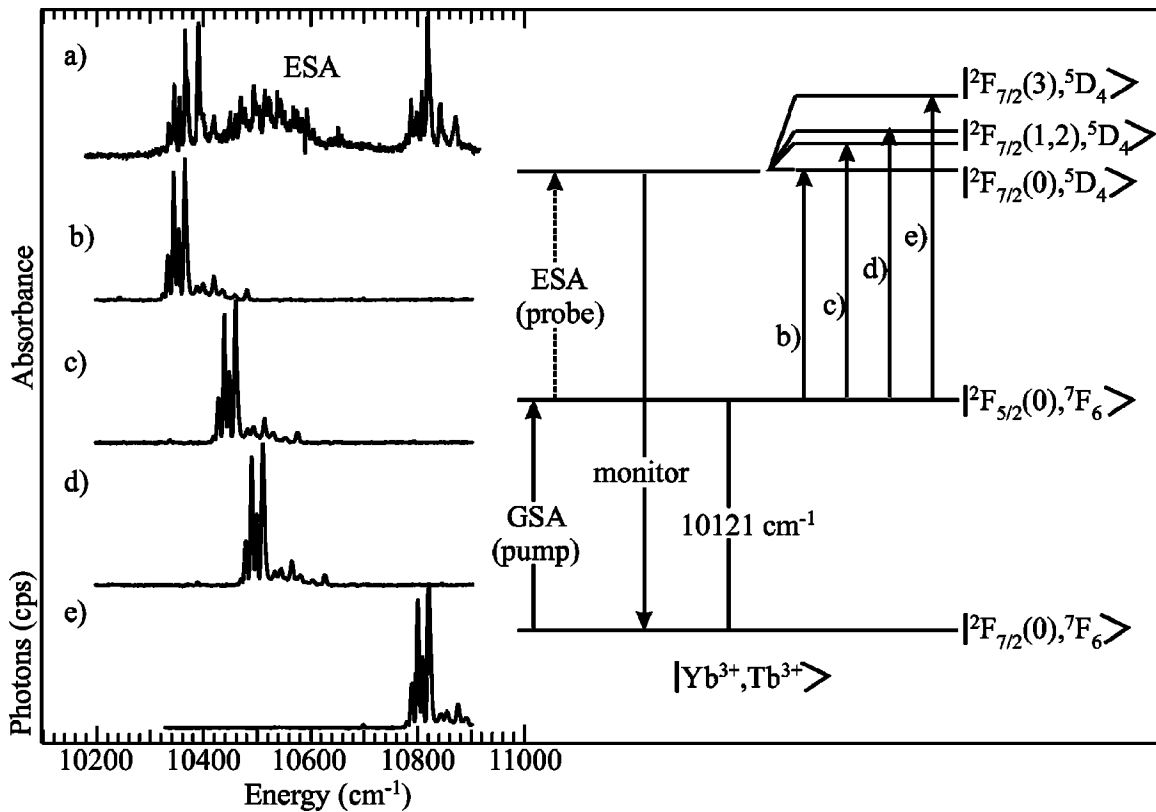


FIG. 8. (a) ESA spectrum at 10 K monitoring luminescence at 18193 cm^{-1} . The pump laser was set to 10121 cm^{-1} with a power of 60 W/mm^2 , while the probe laser was scanned through the appropriate energy region with a power of 0.25 W/mm^2 . The lower traces show the $|{}^2F_{7/2}(0), {}^7F_6(0)\rangle \rightarrow |{}^2F_{7/2}(0), {}^5D_4(j)\rangle$ absorption spectrum at 10 K, shifted in energy by -10121 cm^{-1} (b), $(-10121 + 105) \text{ cm}^{-1}$ (c), $(-10121 + 149) \text{ cm}^{-1}$ (d), and $(-10121 + 454) \text{ cm}^{-1}$ (e). The diagram on the right demonstrates the principle of the measurement and assigns the various parts of the ESA spectrum to Yb^{3+} - Tb^{3+} dimer ESA transitions. Each of arrows (b)–(e) corresponds to an absorption spectrum shown on the left. Note that the crystal field levels of the Yb^{3+} ion are distinguished while only the spin-orbit labels of the Tb^{3+} are included.

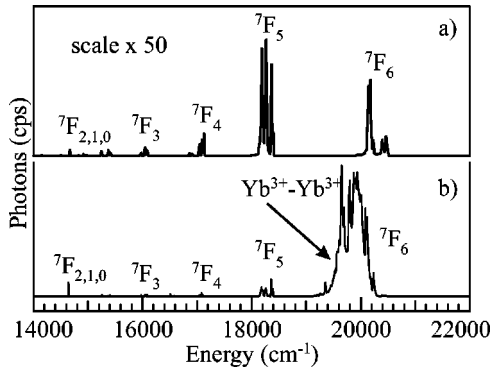


FIG. 9. 10-K UC luminescence spectra with an excitation energy of 10364 cm⁻¹ (a) and 10590 cm⁻¹ (b). In both (a) and (b) the excitation power densities were 53 W/mm².

observed in spectrum (a) in the region from 10300 to 10900 cm⁻¹, and will be discussed in Sec. IV C.

The results of two color excitation experiments at $T = 10$ K, described in Sec. II B, are shown in Fig. 8(a). The Tb³⁺ UC luminescence intensity is plotted in Fig. 8(a) as a function of the probe laser energy, 0.25 W/mm², with the pump laser, 60 W/mm², fixed at the GSA energy of 10121 cm⁻¹. A multitude of lines is found between 10300 and 10900 cm⁻¹. Plotted in trace (b) is the 10 K Tb³⁺ ⁷F₆ → ⁵D₄ absorption spectrum, shifted down in energy by an amount equal to that of the Yb³⁺ ²F_{5/2}(0) level: 10121 cm⁻¹. The energetic positions of the ⁵D₄ crystal field levels, derived from the 10 K absorption spectrum, can be found in Table I. Plots (c), (d), and (e) are the same as b) but displaced higher in energy by amounts equal to the Yb³⁺ ²F_{7/2} ground state crystal field levels: (c) 105 cm⁻¹, (d) 149 cm⁻¹, and (e) 454 cm⁻¹.

The UC luminescence at 10 K are plotted in Fig. 9 for 10364 and 10590-cm⁻¹ NIR excitations in (a) and (b), respectively. The two spectra are clearly different. All transitions in the visible region originate from Tb³⁺ ⁵D₄ and are labeled with the final transition in the Tb³⁺ ⁷F_J manifold except for the broad luminescence around 20000 cm⁻¹ in (b) which is assigned to Yb³⁺-Yb³⁺ cooperative luminescence. Spectrum (a) has been multiplied by 50. The laser power for both experiments was 53 W/mm².

The 10-K excitation spectrum of the 9972-cm⁻¹ Yb³⁺ luminescence, similar to Fig. 7(b), is extended to 14500 cm⁻¹ in Fig. 10. The groups of transitions are labeled in dimer notation neglecting crystal field splittings. The data at energies higher than 11500 cm⁻¹ are multiplied by 2000.

IV. ANALYSIS AND DISCUSSION

Cs₃Tb₂Br₉ crystallizes in the space group $R\bar{3}c$. The Tb³⁺ ions are incorporated as face-sharing dimers separated by 3.89 Å (Fig. 1). The site symmetry for a single Tb³⁺ is C_{3v}. The threefold axis of the dimer coincides with the c axis of the crystal.²⁹ Yb³⁺ dopant ions replace Tb³⁺ host ions. Therefore, the relevant complex for this study is an Yb³⁺-Tb³⁺ dimer, as shown in Fig. 1. With a 1% dopant concentration 99% of all Yb³⁺ ions are incorporated as

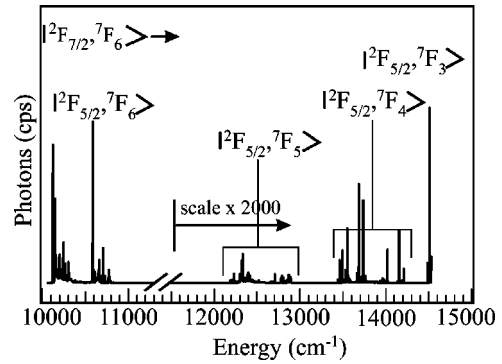


FIG. 10. Excitation spectrum of $|^2F_{5/2}(0), ^7F_6(0)\rangle \rightarrow |^2F_{7/2}(2), ^7F_6(0)\rangle$ luminescence monitored at 9972 cm⁻¹ at 10 K. Assignments for transitions are made in the Yb³⁺-Tb³⁺ dimer notation. The bands higher in energy than 11500 cm⁻¹ are expanded by a factor of 2000.

Yb³⁺-Tb³⁺ dimers with the remaining 1% as Yb³⁺-Yb³⁺ dimers. We will first discuss the energy levels and spectroscopic properties of the RE ions alone (Sec. IV A), before discussing the dimer states, transitions, and UC mechanisms in Secs. IV B and IV C.

A. Single ion levels

The trigonal crystal field (CF) splits all degeneracies except for Kramers. Since the Tb³⁺ has eight electrons in the 4f shell, there are no Kramers doublets, and therefore we observe the maximum number of CF levels in each spin-orbit manifold.³⁰ The nine CF levels of the Tb³⁺ ⁵D₄ excited state, derived from high-resolution absorption spectra, are listed in Table I. Transitions from the lowest CF level of the ⁷F₆ ground state to each of the ⁵D₄ levels are observed in the 10-K absorption spectrum presented in Fig. 8(b). Note that this absorption spectrum has been shifted by 10121 cm⁻¹ for later discussions in Sec. IV C. Also present in this spectrum are hot bands due to transitions from ground state CF levels which are 12 and 21 cm⁻¹ above the ground level. The energetic position of the ⁵D₄ levels is important for later discussions concerning upconversion and dimer transitions, Sec. IV C.

Tb³⁺ ⁵D₄ → ⁷F_J luminescence spectrum is presented in Fig. 3 under 20486-cm⁻¹ excitation at 10 K. Each group of lines has at least $2J+1$ peaks contained in them with some having more due to relatively strong vibronic sidebands, e.g. ⁵D₄ → ⁷F₅. The electronic transitions are typically sharp, app. 1 cm⁻¹ full width at half maximum (FWHM), with the vibronic side band transitions being broader. The identification of transitions corresponding to only one Tb³⁺ species and the single exponential nature of the Tb³⁺ luminescence decay means there is only one Tb³⁺ site.

Yb³⁺ has 13 electrons, and therefore every level is a Kramers doublet, with four in the ²F_{7/2} ground state and three in the ²F_{5/2} excited state. The luminescence spectrum in Fig. 2 allows the assignment of the energetic position of the four CF levels, labeled 0, 1, 2, and 3, of ²F_{7/2} given in Table I.

Dimer Energy Level Diagram

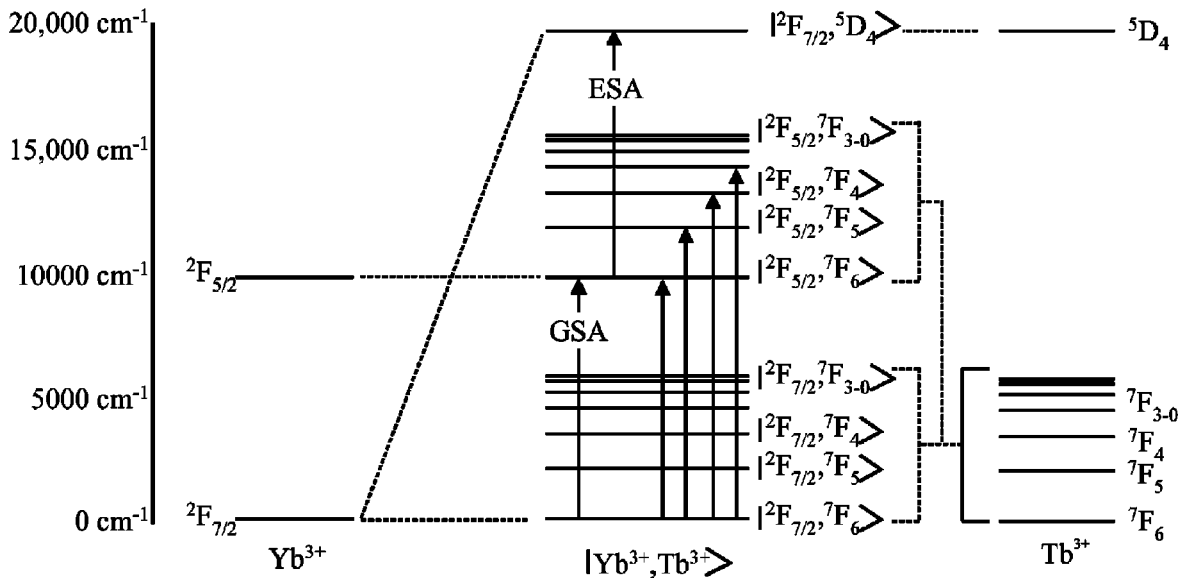


FIG. 11. Energy level diagram of relevant levels of Yb^{3+} (left), Tb^{3+} (right) and the $\text{Yb}^{3+}\text{-Tb}^{3+}$ dimer (middle). For simplicity the crystal field splittings are neglected. The dashed lines demonstrate where the different components of the dimer levels come from. The arrows represent the transitions discussed in the text.

The energies of the three ${}^2F_{5/2}$ crystal field levels, 0, 1, and 2 (Table I) are determined from Fig. 7(b). The energies of the Yb^{3+} levels in $\text{Cs}_3\text{Tb}_2\text{Br}_9$, both in ${}^2F_{7/2}$ and ${}^2F_{5/2}$, are similar to those of $\text{Cs}_3\text{Yb}_2\text{Br}_9$.³¹ As in the case for Tb^{3+} , the luminescence and excitation lines of Yb^{3+} have a FWHM of approximately 1 cm^{-1} . We observe only one site for Yb^{3+} in this host as expected. The additional broader lines, both in the luminescence (Fig. 2) and excitation spectra [Fig. 7(b)], are vibronic side bands on the $(0)\rightarrow(0)$ transition. Some of the sharp lines present in the excitation spectrum of Fig. 7(b), which are not resonant with Yb^{3+} single ion transitions, will be discussed later in Sec. IV C.

B. Upconversion

Excitation at 10590 cm^{-1} leads to visible by eye green Tb^{3+} UC luminescence at all temperatures from 100 to 300 K (Fig. 5). This is remarkable since Tb^{3+} has no energy levels in this region to absorb this radiation. Yb^{3+} does have energy levels in this region, but has no straightforward means of transferring this energy. This is obvious from looking at the single ion levels of Tb^{3+} and Yb^{3+} (Fig. 11). Many papers in the past have reported on this phenomenon in a variety of host.^{15–19,14,20,21} Most researchers attributed this luminescence to a cooperative sensitization mechanism whereby two excited Yb^{3+} ions simultaneously transfer their energy to one Tb^{3+} ion.

We recently studied this process in $\text{SrCl}_2\text{:Yb,Tb}$, and found that phonon assisted cooperative sensitization is the dominant UC mechanism in this host.^{22,23} The integrated UC luminescence was found to increase by more than three orders of magnitude between 10 and 300 K in $\text{SrCl}_2\text{:Yb,Tb}$. Below 100 K for all NIR excitation energies $\text{Yb}^{3+}\text{-Yb}^{3+}$

pair luminescence and luminescence from Er impurities dominated the spectra. Most previous studies were done at room temperature, and therefore did not observe the dramatic quenching of Tb^{3+} UC luminescence at temperatures below 100 K. $\text{Cs}_3\text{Tb}_2\text{Br}_9\text{:Yb}$ is special in that it exhibits clean Tb^{3+} UC luminescence at temperatures down to 10 K (Fig. 5), and with certain excitation energies this emission is clearly the dominant emission (Fig. 9). For excitation around 10590 cm^{-1} into a ${}^2F_{7/2}\rightarrow{}^2F_{5/2}$ GSA of Yb^{3+} the behavior in the title compound is very comparable to $\text{SrCl}_2\text{:Yb,Tb}$ with a similar mechanism at work.

1. Upconversion at high temperatures

As the temperature of $\text{Cs}_3\text{Tb}_2\text{Br}_9\text{:Yb}^{3+}$ is raised from 10 to 300 K the integrated Tb^{3+} UC luminescence intensity increases dramatically, see Fig. 5. The VIS/NIR photon ratio increases from $3.6(10)^{-9}$ at 10 K to $9(10)^{-6}$ at 300 K with Yb^{3+} ${}^2F_{7/2}(0)\rightarrow{}^2F_{5/2}(2)$ excitation at 10590 cm^{-1} . In $\text{SrCl}_2\text{:Yb,Tb}$ we found an increase by more than three orders of magnitude in the same temperature range for the same type of excitation.^{22,23}

One of the standard experimental techniques for determining an UC mechanism is excitation spectroscopy.³ A GSA/ESA mechanism will show peaks in an UC excitation experiment associated with a single GSA step and a single ESA step while a GSA/ETU mechanism will simply follow the square of the GSA for the two photon process we are considering.⁴ Figure 6 displays the VIS Tb^{3+} UC luminescence excitation and the square of the NIR Yb^{3+} luminescence excitation spectrum at 100 K. The two spectra are very similar, and only in the inset can subtle differences between the two be observed. Based on the temperature dependence

and the similarity of the excitation spectra in Fig. 6, we conclude that at 100 K the dominant UC process is a GSA/ETU mechanism involving two ground state absorption steps. We assign the dominant UC mechanism at temperatures above 50 K to the phonon-assisted cooperative sensitization mechanism as in SrCl₂:Tb,Yb.^{22,23} There is a 223-cm⁻¹ energy gap between two times the metastable Yb³⁺ ²F_{5/2}(0) crystal field level and the lowest Tb³⁺ ⁵D₄(0) crystal field level, which is bridged by phonons. We also note from Fig. 5 that with increasing temperature the Yb³⁺-Yb³⁺ cooperative luminescence decreases, suggesting a loss of this intensity to the Tb³⁺ UC luminescence.

The two very weak peaks *a* and *b* observed in the 100-K excitation spectra of Fig. 6 are transitions originating from thermally populated CF levels of the Yb³⁺ ground state, Sec. IV C. Peaks *a* and *b* are 108 and 154 cm⁻¹ lower in energy than the peak at 10590 cm⁻¹, and correspond to transitions from Yb³⁺ ²F_{7/2}(1) and ²F_{7/2}(2) CF levels to Yb³⁺ ²F_{5/2}(2). Peak *c* will be discussed later in Sec. IV C.

2. Upconversion at 10 K

The dominant broad UC emission band around 20000 cm⁻¹ at 10 K in Fig. 5(b) is assigned to cooperative Yb³⁺-Yb³⁺ pair luminescence.³² Tb³⁺ luminescence is app. 100 times weaker than the Yb³⁺-Yb³⁺ cooperative luminescence for excitation at 10590 cm⁻¹ at 10 K. However, at the same temperature but for 10369 cm⁻¹ excitation [Fig. 9(a)], the Yb³⁺-Yb³⁺ cooperative luminescence is suppressed and the Tb³⁺ UC luminescence dominates the VIS spectrum. This will be discussed in more detail in Sec. IV C. The 10-K Tb³⁺ ⁵D₄ lifetime is very similar for direct and UC excitation, see Fig. 4 and Table II. While direct excitation into the ⁵D₄ level excites all Tb³⁺ ions, UC excitation excites preferentially those Tb³⁺ ions incorporated as an Yb³⁺-Tb³⁺ pair. Since there is no difference in the luminescence spectra or lifetime of the two separate species, this shows that the Tb³⁺ ions which are located next to the Yb³⁺ ions have very small differences in the local crystal field compared with those located next to another Tb³⁺ ion.³³ This is in contrast to other lattices for which it was found that the ⁵D₄ level of the upconversion active subset of Tb³⁺ ions had a shorter lifetime than the bulk ions.^{23,16,17,34}

The 10 K UC luminescence excitation spectrum in Fig. 7(a) clearly shows that this spectrum is not the square of the GSA spectrum [Fig. 7(b)]. The only common electronic origin seen in these plots corresponds to the ²F_{7/2}(0) → ²F_{5/2}(2) transition located at 10590 cm⁻¹. The two remarkable features of the 10 K UC luminescence excitation spectrum in Fig. 7(a) are the following: (i) the ²F_{7/2}(0) → ²F_{5/2}(0) and ²F_{7/2}(0) → ²F_{5/2}(1) GSA transitions of Yb³⁺ are completely absent; and (ii) numerous additional peaks not present in the GSA spectrum of Fig. 7(b) are found from 10300 to 10900 cm⁻¹. These additional peaks are due to an ESA, and will be discussed in Sec. IV C.

From simple energy conservation, the lowest level of Tb³⁺ ⁵D₄, 20465 cm⁻¹ (Table I), cannot be reached at 10 K by two photons with energies of 10121 and 10148 cm⁻¹,

corresponding to the ²F_{5/2}(0) and (1) levels of Yb³⁺, respectively. However, two photons resonant with the Yb³⁺ ²F_{7/2}(0) → ²F_{5/2}(2) transition at 10590 cm⁻¹ have enough energy to reach the lowest Tb³⁺ ⁵D₄ level.

C. GSA/ESA mechanism in the Yb³⁺-Tb³⁺ dimer

Recent publications from this group presented upconversion of NIR radiation resonant with Yb³⁺ GSA transitions to VIS luminescence of Mn²⁺ in a variety of ternary Mn²⁺ halide lattices.^{6,7,11,8-10} In some systems short pulse excitation into the Yb³⁺ absorption region led to an immediate decay of the Mn²⁺ UC luminescence intensity, indicating a GSA/ESA sequence. Additionally, two color experiments were performed which directly revealed the ESA transition. These results were explained by considering an exchange interaction between Yb³⁺ and Mn²⁺ ions which provides intensity to the ESA step via the Tanabe mechanism.³⁵

An exchange induced mechanism has also been suggested to account for the unusual ²E → ⁴A₂ emission in Cr³⁺ doped EuAlO₃.^{36,37} In addition to the normal *R*-line emission there are lines in the NIR. The energy difference between these and the *R* lines correspond to the energy differences between the Eu³⁺ ⁷F₀ ground state multiplet and the ⁷F_{*J*}(*J*=1-6) excited state multiplets. The process was found to be very efficient, and some of the lines are more intense than the *R* lines. A mechanism based on multipole-multipole interactions was therefore ruled out.

To establish the UC mechanism in this host at 10 K we consider the following facts. From Sec. IV B any mechanism involving a GSA step followed by an ETU step is eliminated, leaving only a GSA/ESA mechanism as a possibility. Clearly this must be a cooperative process between the Yb³⁺ and Tb³⁺ ions. An exchange interaction for rare-earth ions in this lattice is well established.^{24,25} The effectiveness of an exchange interaction in mixed GSA/ESA driven UC systems has also been established.⁶⁻¹¹ Therefore, based on the previous facts, we propose that the observed upconversion to the Tb³⁺ ⁵D₄ state at 10 K is based on an exchange mechanism, similar to the examples given above, within the YbTbBr₉³⁻ dimer.

Since we are dealing with an undiluted Tb compound, 99% of all Yb³⁺ ions are present in these units. The Hamiltonian for the Yb³⁺-Tb³⁺ dimer is then written

$$\tilde{H}_{Yb,Tb} = \tilde{H}_{Yb} + \tilde{H}_{Tb} + \tilde{H}_{ex}(Yb,Tb), \quad (1)$$

The first two terms are the single ion Hamiltonians. The last term stands for the exchange interactions. Without this term the wave functions are simply those corresponding to the single ion Hamiltonians, e.g., Yb³⁺ ²F_{7/2}(0) and Tb³⁺ ⁷F₆(0) for the ground levels of each of the two ions. However, these are no longer proper eigenstates when $\tilde{H}_{ex}(Yb,Tb)$ is nonzero. The proper dimer states carry a double label, |Yb³⁺ ²F_{7/2}(0), Tb³⁺ ⁷F₆(0)⟩ e.g., for the lowest level of the dimer ground state. The diagrams in Figs. 7, 8, and 11 use this notation, often without specifying the CF level.

For one-color excitation the minimum energy required for a sequence of GSA and ESA steps is 10344 cm^{-1} , i.e., the energy difference between $|^2F_{7/2}(0), ^5D_4(0)\rangle$ and $|^2F_{5/2}(0), ^7F_6(0)\rangle$. This is exactly the energy at which the 10 K one-color UC excitation spectrum in Fig. 7(a) begins. In fact the first set of peaks in Fig. 7(a) are exactly coincident in energy with the $|^2F_{7/2}(0), ^5D_4(j)\rangle$ energy levels when shifted down by an amount equal to the $|^2F_{5/2}(0), ^7F_6(0)\rangle$ energy of 10121 cm^{-1} , i.e., they correspond to ESA transitions within the dimer.

A two-color excitation experiment provided the key to understanding the UC mechanism at 10 K in the title system. The detailed description of the experiment is in Sec. II B. The UC luminescence intensity at 10 K, as a function of probe beam energy for a fixed GSA pump beam energy of 10121 cm^{-1} , is given in Fig. 8(a). Many of the lines which were observed in the one-color excitation spectrum [Fig. 7(a)] are also observed in this two-color excitation spectrum. However, the most prominent peak in Fig. 7(a), corresponding to the $|^2F_{7/2}(0), ^7F_6(0)\rangle \rightarrow |^2F_{5/2}(2), ^7F_6(0)\rangle$ transition, is absent in Fig. 8(a). This is because the probe beam in the two-color experiment scans the ESA transitions from the metastable $|^2F_{5/2}(0), ^7F_6(0)\rangle$ dimer level to the multitude of $|^2F_{7/2}(i), ^5D_4(j)\rangle$ dimer levels, where $i=0 \rightarrow 3$ and $j=0 \rightarrow 8$, and therefore does not involve the $|^2F_{7/2}(0), ^7F_6(0)\rangle \rightarrow |^2F_{5/2}(2), ^7F_6(0)\rangle$ transition. This is represented schematically in Fig. 8. There are $4 \times 9 = 36$ possible electronic dimer transitions. For simplicity, in the diagram on the right, we neglect the CF splitting of $\text{Tb}^{3+} ^5D_4$ but consider the four CF levels of $\text{Yb}^{3+} ^2F_{7/2}$. Each of the ESA arrows in Fig. 8 then represents nine transitions from the $|^2F_{5/2}(0), ^7F_6(0)\rangle$ level to the CF levels of $|^2F_{7/2}(i), ^5D_4(j)\rangle$, where $i = 0, 1, 2, 3$ corresponds to the arrows (b), (c), (d), and (e), respectively.

To help explain this graphically we have plotted the GSA spectrum of the $|^2F_{7/2}(0), ^7F_6(0)\rangle \rightarrow |^2F_{7/2}(0), ^5D_4(j)\rangle$ transitions in Figs. 8(b)–8(e). Each has been shifted down by the energy difference between $|^2F_{5/2}(0), ^7F_6(0)\rangle$ and $|^2F_{7/2}(i), ^7F_6(0)\rangle$ levels. Figures 8(b)–8(e) are then the putative dimer ESA spectra broken into four groups, corresponding to $i=0 \rightarrow 3$, respectively. There is an exact match of energy for each of the lines in Fig. 8(a) with the lines in Figs. 8(b)–8(e). This remarkable result allows the unambiguous assignment of the spectrum in Fig. 8(a) to $|^2F_{5/2}(0), ^7F_6(0)\rangle \rightarrow |^2F_{7/2}(i), ^5D_4(j)\rangle$ dimer ESA transitions. The intensity ratios are of course different, because Figs. 8(b)–8(e) correspond to transitions originating from a different level, $|^2F_{7/2}(0), ^7F_6(0)\rangle$, than Fig. 8(a), $|^2F_{5/2}(0), ^7F_6(0)\rangle$.

The energy level diagram in Fig. 11 shows that, neglecting CF splitting, there are six dimer states higher in energy than $|^2F_{5/2}, ^7F_6\rangle$ but lower than $|^2F_{7/2}, ^5D_4\rangle$. Figure 10 displays a 10-K Yb^{3+} luminescence excitation spectrum taken by scanning a $\text{Ti:Al}_2\text{O}_3$ laser from 10000 to 14500 cm^{-1} , and monitoring $|^2F_{5/2}(0), ^7F_6(0)\rangle \rightarrow |^2F_{7/2}(2), ^7F_6(0)\rangle$ emission at 9972 cm^{-1} . As in Fig. 7(a), two groups of intense peaks separated by 460 cm^{-1} in the region between 10000 and 11000 cm^{-1} are observed corresponding to $|^2F_{7/2}(0), ^7F_6(0)\rangle \rightarrow |^2F_{5/2}(0,1), ^7F_6(0)\rangle$ and

$|^2F_{7/2}(0), ^7F_6(0)\rangle \rightarrow |^2F_{5/2}(2), ^7F_6(0)\rangle$ transitions. These are the transitions also observed in the absorption spectrum of Yb^{3+} single ions in this CF environment.³¹ Between 12000 and 14600 cm^{-1} much weaker peaks are observed which correspond to dimer transitions involving a label change for both Yb^{3+} and Tb^{3+} ; see Fig. 10. Similar cooperative absorption has been observed for homogeneous dimer pairs such as in PrCl_3 where the cooperative action between two Pr^{3+} ions was attributed to a Coulombic interaction.³⁸ The data in Fig. 10 are grouped and labeled according to transitions ending on different spin-orbit levels of $\text{Tb}^{3+} ^7F_j$. Notice that within each group we observe the same separation of 460 cm^{-1} into two subgroups as between 10000 and 11000 for the strong peaks. The many peaks within the groups correspond to the crystal field split levels $|^2F_{5/2}(i), ^7F_{6 \rightarrow 3}(j)\rangle$.

Evidence of dimer transitions is also found in the region between 10000 and 11000 cm^{-1} where extra peaks are found which are assigned to dimer transitions such as $|^2F_{7/2}(0), ^7F_6(0)\rangle \rightarrow |^2F_{5/2}(1), ^7F_6(j)\rangle$, where $j \neq 0$. Other evidence is found in Fig. 6, where peak *c* cannot be associated with only an Yb^{3+} ion. This line is assigned to a hot absorption transition, $|^2F_{7/2}(0), ^7F_6(1)\rangle \rightarrow |^2F_{5/2}(2), ^7F_6(0)\rangle$.

Excitation into the $|^2F_{5/2}(i), ^7F_{5 \rightarrow 3}(j)\rangle$ dimer states between 12000 and 14500 cm^{-1} , (Fig. 10) at 10 K does not lead to any detectable UC luminescence. This is explained by the absence of any excited states between $10121 + (12000-14500) \cong 22121-24621 \text{ cm}^{-1}$. The next higher state, $|^2F_{7/2}(0), ^5D_3(0)\rangle$, is expected above 26000 cm^{-1} .

It is also interesting that no $|^2F_{5/2}(0), ^7F_5(0)\rangle \rightarrow |^2F_{7/2}(i), ^7F_6(j)\rangle$ luminescence was observed upon 10 K $|^2F_{7/2}(0), ^7F_6(0)\rangle \rightarrow |^2F_{5/2}(i), ^7F_5(j)\rangle$ excitation at 12332 cm^{-1} . There are two explanations for the lack of this luminescence. First, the energy gap between $|^2F_{5/2}, ^7F_5\rangle$ and $|^2F_{5/2}, ^7F_6\rangle$ (see Fig. 11) corresponds to 6.3 highest energy phonons. Usually in lanthanides this is large enough for radiative *f-f* transitions to successfully compete against non-radiative multiphonon relaxation.³⁹ But in our case the radiative $|^2F_{5/2}(0), ^7F_5(0)\rangle \rightarrow |^2F_{7/2}(i), ^7F_6(j)\rangle$ transition involves a change of both dimer labels. As seen in Fig. 10 these have typically four orders of magnitude weaker oscillator strengths and therefore the nonradiative relaxation dominates. Second, the dimer can undergo the radiative $|^2F_{5/2}(0), ^7F_5(0)\rangle \rightarrow |^2F_{7/2}(i), ^7F_5(0)\rangle$ transition followed by a multiphonon or radiative relaxation to the ground state. In both cases the only observable luminescence occurs via a label change of only the Yb^{3+} ion.

V. CONCLUSIONS

Visible by eye green Tb^{3+} UC luminescence is reported for the title compound down to 10 K. Conclusive data are presented which demonstrate a cooperative GSA/ESA mechanism responsible for this UC luminescence at 10 K. We explain this result in terms of an Yb^{3+} - Tb^{3+} dimer coupled by an exchange interaction. Transitions involving a change on both ions of the dimer typically have four orders of magnitude smaller oscillator strengths than transitions in-

volving only one label change. The latter are essentially single-ion transitions.

The cooperative GSA/ESA mechanism for upconversion within an exchange coupled system has only recently been discovered. The system presented in this paper clearly demonstrates this mechanism for a RE-RE pair of unequal ions. Other papers have looked at Yb³⁺-Mn²⁺ and Yb³⁺-Cr³⁺ systems, some of which are very efficient. In the present Yb-Tb dimer this mechanism can clearly be observed and characterized only at low temperatures. At

100 K and above the cooperative sensitization mechanism, which is typically 10³ times more efficient, dominates the UC behavior.

ACKNOWLEDGMENTS

The authors thank Oliver Wenger for many interesting discussions. Thanks also to Karl Krämer and Daniel Biner for assistance in growing the crystals. This work was supported by the Swiss National Science Foundation.

-
- ¹F. Auzel, C.R. Acad. Sci. Paris, **262**, 1016 (1966).
²W. Lenth and R. M. Macfarlane, Opt. Photonics News **3**, 8 (1992).
³F. Auzel, J. Lumin. **45**, 341 (1990).
⁴D. R. Gamelin and H. U. Güdel, Top. Curr. Chem. **214**, 1 (2001).
⁵V. V. Ovsyankin and P. P. Feofilov, Pis'ma Zh. Éksp. Teor. Fiz. **4**, 471 (1966) [JETP Lett. **4**, 317 (1966)].
⁶R. Valiente, O. S. Wenger, and H. U. Güdel, Chem. Phys. Lett. **320**, 639 (2000).
⁷R. Valiente, O. S. Wenger, and H. U. Güdel, Phys. Rev. B **63**, 165102 (2001).
⁸P. Gerner, O. S. Wenger, R. Valiente, and H. U. Güdel, Inorg. Chem. **40**, 4534 (2001).
⁹C. Reinhard, P. Gerner, R. Valiente, O. S. Wenger, and H. U. Güdel, J. Lumin. **94-95**, 331 (2001).
¹⁰C. Reinhard, R. Valiente, and H. U. Güdel, J. Phys. Chem. B **106**, 10 051 (2002).
¹¹R. Valiente, O. S. Wenger, and H. U. Güdel, J. Chem. Phys. **116**, 5196 (2002).
¹²G. H. Dieke *Spectra and Energy Levels of Rare Earth Ions in Crystals* (Interscience, New York, 1968).
¹³V. I. Bilak, G. M. Zverev, G. O. Karapetyan, and A. M. Onischenko, Pis'ma Zh. Éksp. Teor. Fiz. **14**, 301 (1971) [JETP Lett. **14**, 199 (1971)].
¹⁴M. A. Noginov, P. Venkateswarlu, and M. Mahdi, J. Opt. Soc. Am. B **13**, 735 (1996).
¹⁵L. D. Livanova, I. G. Saitkulov, and A. L. Stolov, Fiz. Tvera. Tela (Leningrad) **11**, 918 (1969) [Sov. Phys. Solid State **11**, 750 (1969)].
¹⁶F. W. Ostermayer and L. G. VanUitert, Phys. Rev. B **1**, 4208 (1970).
¹⁷B. M. Antipenko, A. V. Dmitryuk, G. O. Karapetyan, U. S. Zubkova, V. I. Kosyakov, A. A. Mak, and N. V. Mishailova, Opt. Spektrosk. **35**, 540 (1973) [Opt. Spectrosc. **35**, 315 (1973)].
¹⁸R. S. Brown, W. S. Brocklesby, W. L. Barnes, and J. E. Townsend, J. Lumin. **63**, 1 (1995).
¹⁹J. L. Adam, N. Duhamel-Henry, and J. Y. Allain, J. Non-Cryst. Solids **213-214**, 245 (1997).
²⁰W. Strek, P. Deren, and A. Bednarkiewicz, J. Lumin. **87-89**, 999 (2000).
²¹I. R. Martín, A. C. Yáñez, J. Mendez-Ramos, M. E. Torres, and V. D. Rodriguez, J. Appl. Phys. **89**, 2520 (2001).
²²G. M. Salley, R. Valiente, and H. U. Güdel, J. Lumin. **94-95**, 305 (2001).
²³G. M. Salley and H. U. Güdel, J. Phys.: Condens. Matter **14**, 5461 (2002).
²⁴A. Furrer, H. U. Güdel, H. Blank, and A. Heidemann, Phys. Rev. Lett. **62**, 210 (1989).
²⁵H. U. Güdel, A. Furrer, and H. Blank, Inorg. Chem. **29**, 4081 (1990).
²⁶Ph. Goldner, F. Pellé, D. Meichenin, and F. Auzel, J. Lumin. **71**, 137 (1997).
²⁷J. B. Reed, B. S. Hopkins, and L. F. Audrieth, Inorg. Synth. **1**, 28 (1936).
²⁸G. Meyer, Inorg. Synth. **25**, 146 (1989).
²⁹A. Dönni, A. Furrer, and H. Güdel, J. Solid State Chem. **81**, 278 (1989).
³⁰B. Henderson and G. F. Imbusch, *Optical Spectroscopy of Inorganic Solids* (Oxford University Press, Clarendon, Oxford, 1989).
³¹M. P. Hehlen and H. U. Güdel, J. Chem. Phys. **98**, 1768 (1993).
³²E. Nakazawa and S. Shiyona, Phys. Rev. Lett. **25**, 1710 (1970).
³³D. R. Gamelin and H. U. Güdel, Inorg. Chem. **38**, 5154 (1999).
³⁴W. Strek, A. Bednarkiewicz, and P. J. Deren, J. Lumin. **92**, 229 (2001).
³⁵J. Ferguson, H. J. Guggenheim, and Y. Tanabe, J. Phys. Soc. Jpn. **21**, 692 (1966).
³⁶J. P. van der Ziel and L. G. van Uitert, Phys. Rev. B **1**, 4208 (1970).
³⁷J. P. van der Ziel and L. G. van Uitert, Phys. Rev. B **8**, 1889 (1973).
³⁸F. Varsanyi and G. H. Dieke, Phys. Rev. Lett. **7**, 442 (1961).
³⁹T. C. Brunold and H. U. Güdel, in *Inorganic Electronic Structure and Spectroscopy*, edited by E. I. Solomon and A. B. Lever (Wiley, New York, 1999), pp. 259–306.